The Meteoritical Society

Meteoritics & Planetary Science 42, Nr 7/8, 1267–1279 (2007)
Abstract available online at http://meteoritics.org

^{36}Cl, ^{26}Al, and O isotopes in an Allende type B2 CAI: Implications for multiple secondary alteration events in the early solar system

Takayuki USHIKUBO[1*†], Yunbin GUAN[1††], Hajime HIYAGON[2], Naoji SUGIURA[2], and Laurie A. LESHIN[1†††]

[1]Department of Geological Sciences, Arizona State University, Tempe, Arizona 85287, USA
[2]Department of Earth and Planetary Science, University of Tokyo, 7-3-1 Hongo, Bunkyo, Tokyo 113-0033 Japan
[†]Present address: Department of Geology and Geophysics, University of Wisconsin–Madison, 1215 West Dayton Street, Madison, Wisconsin 53706, USA
[††]Present address: Division of Geological and Planetary Sciences, California Institute of Technology, Pasadena, California 91125, USA
[†††]Present address: Sciences and Exploration Directorate, Goddard Space Flight Center, NASA, Greenbelt, Maryland 20771, USA
[*]Corresponding author. E-mail: ushi@geology.wisc.edu

(Received 12 October 2006; revision accepted 22 April 2007)

Abstract–We measured ^{36}Cl-^{36}S and ^{26}Al-^{26}Mg systematics and O isotopes of secondary phases in a moderately altered type B2 CAI (CAI#2) from the Allende CV3 chondrite. CAI#2 has two distinct alteration domains: the anorthite-grossular (An-Grs) domain that mostly consists of anorthite and grossular, and the Na-rich domain that mostly consists of sodalite, anorthite, and Fe-bearing phases. Large ^{36}S excesses (up to ~400‰) corresponding to an initial ^{36}Cl/^{35}Cl ratio of $(1.4 \pm 0.3) \times 10^{-6}$ were observed in sodalite of the Na-rich domain, but no resolvable ^{26}Mg excesses were observed in anorthite and sodalite of the Na-rich domain (the initial ^{26}Al/^{27}Al ratio $< 4.4 \times 10^{-7}$). If we assume that the ^{36}Cl-^{36}S and the ^{26}Al-^{26}Mg systematics were closed simultaneously, the ^{36}Cl/^{35}Cl ratio would have to be on the order of $\sim 10^{-2}$ when CAIs were formed. In contrast to sodalite in Na-rich domain, significant ^{26}Mg excesses (up to ~35‰) corresponding to an initial ^{26}Al/^{27}Al ratio of $(1.2 \pm 0.2) \times 10^{-5}$ were identified in anorthite of the An-Grs domain. The ^{26}Al-^{26}Mg systematics of secondary phases in CAI#2 suggest that CAIs experienced multiple alteration events. Some of the alteration processes occurred while ^{36}Cl (half-life is 0.3 Myr) and ^{26}Al (half-life is 0.72 Myr) were still alive, whereas others took place much later. Assuming that ^{26}Al was homogeneously distributed in the solar nebula, our study implies that alteration of CAIs occurred as early as within 1.5 Myr of CAI formation and as late as 5.7 Myr after.

INTRODUCTION

Calcium-aluminum-rich inclusions (CAIs) consist of Al, Ca-rich phases such as spinel, melilite, anorthite, and fassaïte (e.g., Grossman 1975). Their bulk chemistry and mineralogy indicate that they are products of high-temperature condensation under solar nebular conditions (Grossman 1972; Wood and Hashimoto 1993; Yoneda and Grossman 1995). CAIs have the oldest Pb-Pb ages of solar system objects (4567.2 ± 0.6 Ma) (Amelin et al. 2002) and most of them show distinct isotopic anomalies, i.e., ^{16}O enrichment of ~50‰ (Clayton 2003) and ^{26}Mg excess from the decay of ^{26}Al (MacPherson et al. 1995). All these characteristics suggest that CAIs were formed by high-temperature processes that occurred at the very early stage of solar system formation when oxygen isotopic heterogeneity existed and short-lived nuclides were still alive.

In addition to high-temperature minerals, CAIs also contain fine-grained and volatile-element-rich phases such as grossular, anorthite, sodalite, and nepheline, which are believed to be formed by later low-temperature secondary alteration processes, i.e., decomposition of primordial phases and introduction of volatile elements such as Fe, Na, and Cl (Wark 1981; Hashimoto and Grossman 1987; McGuire and Hashimoto 1989). These minerals are commonly referred to as secondary phases, in contrast to the primary minerals that crystallized at CAI formation.

Compared to CAI primary minerals, secondary phases are usually ^{16}O-depleted (Clayton et al. 1977; Hiyagon 1998; Aléon et al. 2002; Imai and Yurimoto 2003). In addition, unlike most primary phases that have ^{26}Mg excesses indicating the former existence of live ^{26}Al at $(^{26}\text{Al}/^{27}\text{Al})_0 = 5$ to 6×10^{-5} (MacPherson et al. 1995; Young et al. 2005), most secondary phases contain no resolvable ^{26}Mg excesses

(Hutcheon and Newton 1981; Caillet et al. 1993; Davis et al. 1994; MacPherson et al. 1995; Lin et al. 2005; Hsu et al. 2006). Therefore, secondary alteration processes occurred in an environment that was depleted in ^{16}O and live ^{26}Al.

The temporal and spatial settings of secondary alteration at the early stage of the solar system evolution, however, are still debatable issues. Evidence from the texture and mineralogy of secondary phases in CAIs argues for alteration processes in the solar nebula (Wark 1981; Hashimoto and Grossman 1987; McGuire and Hashimoto 1989; Davis et al. 1994). On the other hand, a positive correlation between metamorphic grade of chondrites and the degree of alteration of CAIs (Kojima et al. 1995), and a wide range of ^{129}I-^{129}Xe ages (>5 Myr) (Swindle 1998) of sodalite in CAIs suggest that secondary alteration processes also occurred in an asteroidal setting.

To better understand secondary alteration processes in the early solar system, in this work we measured ^{36}Cl-^{36}S systematics, ^{26}Al-^{26}Mg systematics, and O isotopes of secondary phases in a moderately altered type B2 CAI (CAI#2) from the Allende CV3 chondrite. ^{36}Cl-^{36}S systematics are based on the decay of ^{36}Cl to ^{36}S (1.9%, ε and β^+; the other decay product is ^{36}Ar, 98.1%, β^-) with a half-life of 0.3 Myr. Recently, evidence for live ^{36}Cl corresponding to initial $^{36}Cl/^{35}Cl$ ratio of (4 to 5) × 10^{-6} was observed in sodalite of some CAIs and a chondrule (Lin et al. 2005; Hsu et al. 2006; Nakashima et al. 2006). Although the initial $^{36}Cl/^{35}Cl$ ratio when CAIs formed has not been determined, ^{36}Cl-^{36}S systematics may provide chronological implications on secondary alteration of CAIs, especially when combined with the study of ^{26}Al-^{26}Mg systematics (half-life ~0.72 Myr) in the same object. In addition, oxygen isotopes of secondary phases could offer further constraints on the alteration processes in the early solar system.

SAMPLE DESCRIPTION

CAI#2 (~5 mm in size) is a type B2 CAI from the Allende CV3 meteorite. The primary phases of CAI#2 are fassaïte, melilite, and spinel (Fig. 1a). The bulk of this CAI consists of large (>200 μm) melilite and fassaïte grains that poikilitically enclose small (~10 μm) spinel grains. Melilite grains are chemically zoned, with åkermanite content increasing from the center to the edge. Fassaïte grains also have igneous zoning and are enriched in Ti and Al in the center of the grains (Table 1). The number density of enclosed spinel grains in fassaïte tends to be higher than that in melilite. The Wark-Lovering rim of this CAI consists of a thin (<5 μm) diopside layer and a thin (<5 μm) spinel layer. The rim structure is partly difficult to identify because it is replaced by secondary phases such as anorthite and sodalite.

CAI#2 is a moderately altered CAI, containing more than 20% secondary phases. There are two distinct types of alteration domains in CAI#2: 1) the anorthite-grossular (An-Grs) domain and 2) the Na-rich domain. Although both domains contact with each other in places, their petrology and distribution in CAI#2 are distinct.

The An-Grs domain, which was observed along the grain boundaries of melilite and fassaïte in the CAI interior (Figs. 1b and 1c), consists mostly of anorthite and grossular. A small amount of monticellite was also observed with grossular. Anorthite has ragged or lath shape and was observed inside or along the edge of the domain. Anorthite that is along the edge tends to be lath-shaped (<50 μm in width) and coarser than that inside the domain. Porous grossular fills the interstices of anorthite grains. Small amounts of spinel, melilite, and fassaïte, which are presumably relicts of primary phases, were also observed in the An-Grs domain.

The Na-rich domain, occurring along the edge of CAI#2 (Figs. 1d and 1e), consists of sodalite, anhedral anorthite, and Fe-bearing phases (spinel and Mg, Si-rich, Ca-free phase, which is presumably olivine). Minor nepheline was also observed around sodalite. There are two different occurrences of sodalite. The majority of sodalite is anhedral and fine-grained, which coexists with fine-grained (typically a few μm) Fe-bearing phases and is commonly observed in the interior of CAI#2. These phases tend to form nodules in a small area (typically ~100 μm in size). These nodules were commonly observed at the inner edge of the Na-rich domain, 50 to 200 μm from the rim of CAI#2. The remaining sodalite grains are subhedral to euhedral grains that scarcely coexist with Fe-bearing phases and are distributed along cracks within CAI#2. An anomalously large euhedral isolated sodalite grain (~40 μm) was identified in a hedenbergite-rich cavity nearby the rim of CAI#2 (Fig. 1e). Anhedral anorthite and primary phases (mostly melilite and spinel) were commonly observed between sodalite-rich nodules and the rim of CAI#2 (Fig. 1d). Minor fine-grained grossular coexists in this area as well (Fig. 1e). Although the anhedral anorthite does not contain detectable Na_2O (Table 1), we regard it as a part of the Na-rich domain because it mostly occurs around the sodalite-rich nodule, and the shapes and sizes of these grains are distinct from those of anorthite observed in the An-Grs domain.

The boundary between the An-Grs and the Na-rich domains is ambiguous. Both domains are in direct contact with primary phases at some places and with each other at other places. However, the Na-rich domain consistently appears more altered than the An-Grs domain because it is observed along the edge of CAI#2 and is more enriched in volatile elements (e.g., Na, Cl) than the An-Grs domain.

EXPERIMENTAL

Petrologic examination and mineral chemistry analysis of CAI#2 were performed using a JEOL JSM-5310 scanning electron microscope (SEM) at the University of Tokyo with a 20 kV beam of 30 pA. X-ray spectra were collected with a

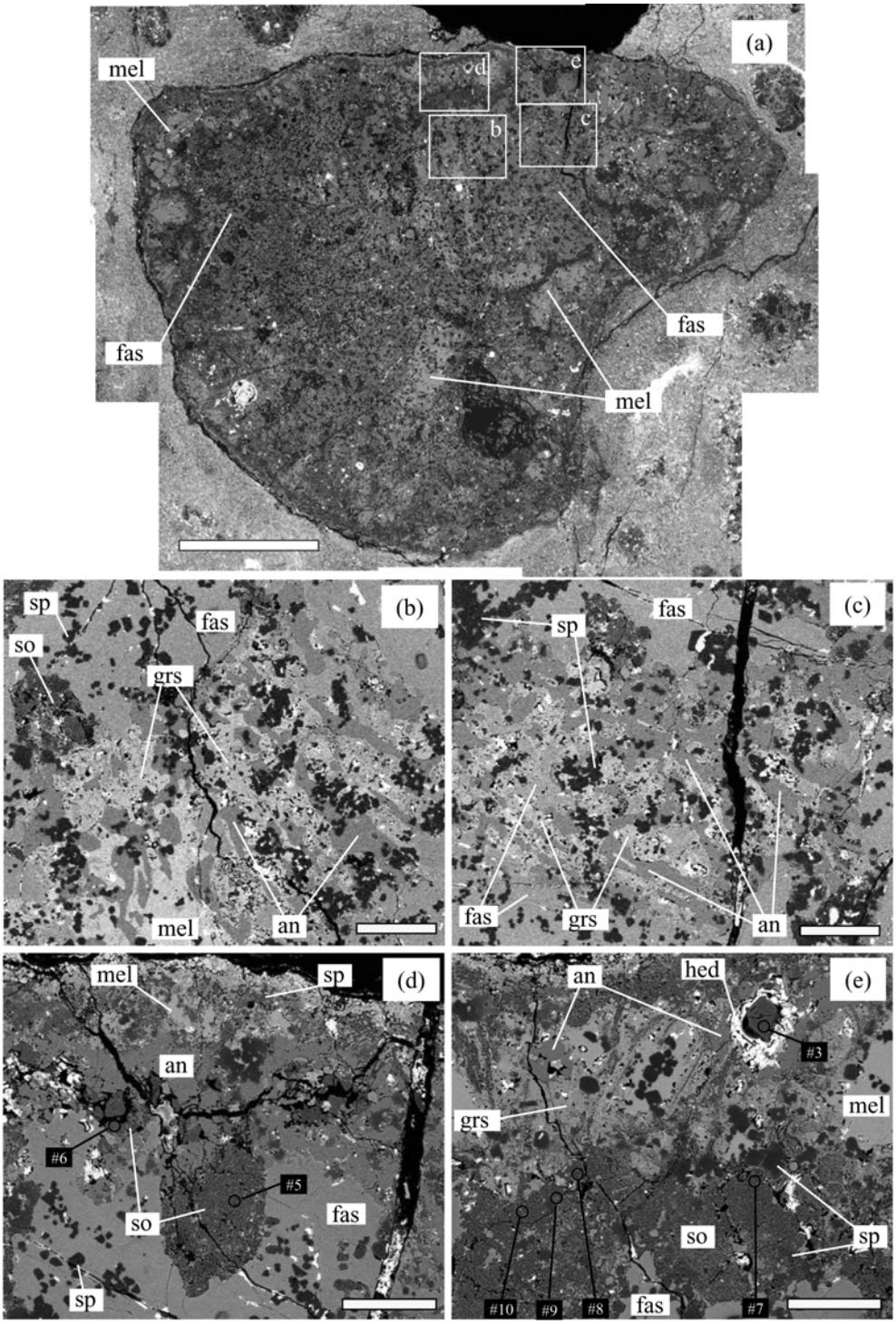

Fig. 1. Backscattered electron image of CAI#2 from the Allende CV3 chondrite. a) Overall image of CAI#2. This CAI consists mainly of melilite (mel), fassaïte (fas), and tiny spinel grains. Four altered parts are outlined and shown in detail in (b–e). b) Image of an anorthite-grossular (An-Grs) domain. Porous grossular fills the interstices of ragged or lath-shaped anorthite grains. This domain was observed on the grain boundary of melilite and fassaïte in the CAI interior. c) Another image of an An-Grs domain. Minor residual melilite exists in this domain. d) Image of a Na-rich domain, consisting mainly of sodalite and anorthite. Sodalite often includes tiny Fe-bearing spinel and silicate grains. This domain was observed along the edge of CAI#2 and sodalite grains tend to be enclosed by anhedral anorthite. e) Another image of a Na-rich domain. Some sodalite grains are in direct contact with grossular or the rim. An anomalously large euhedral sodalite grain (#3, ~40 μm in diameter) was identified in a hedenbergite-rich cavity. Positions of ion probe pits for the ^{36}Cl-^{36}S systematics are shown by white characters on a black background. The scale bar in (a) indicates 1 mm and those in (b–e) indicate 100 μm. Mineral abbreviations: mel = melilite, fas = fassaïte, sp = spinel, an = anorthite, grs = grossular, and so = sodalite.

Table 1. Major element compositions of minerals in CAI#2.

Phase	Melilite		Fassaïte		Spinel	Spinel	Spinel	Grossular	Anorthite	Anorthite
Location	(Center)[a]	(Edge)[b]	(Center)[a]	(Edge)[b]		An-Grs	Na-rich	An-Grs	An-Grs	Na-rich
Na_2O	n.d.	n.d.	n.d.	n.d.	n.d.	n.d.	n.d.	n.d.	n.d.	n.d.
MgO	6.5	7.1	9.9	12.2	29.4	29.6	27.1	1.4	0.2	n.d.
Al_2O_3	21.7	19.2	21.2	15.0	69.4	69.8	68.2	23.0	36.6	36.9
SiO_2	31.0	32.8	39.9	43.8	n.d.	n.d.	n.d.	39.7	42.5	43.0
CaO	40.8	40.9	25.3	25.2	n.d.	0.2	0.2	36.1	20.1	20.3
TiO_2	n.d.	n.d.	4.0	4.7	0.2	n.d.	0.3	n.d.	n.d.	n.d.
V_2O_5	n.d.	n.d.	n.d.	n.d.	0.2	0.3	0.3	n.d.	n.d.	n.d.
Cr_2O_3	n.d.	n.d.	n.d.	n.d.	0.3	0.4	0.2	n.d.	n.d.	n.d.
FeO	n.d.	n.d.	n.d.	n.d.	0.3	n.d.	3.5	n.d.	n.d.	n.d.
Total	100.0	100.1	100.3	100.8	99.7	100.3	99.8	100.1	99.4	100.2

[a]Center of the same grain.
[b]Edge of the same grain.
n.d. = not detected.

Link-ISIS energy dispersive X-ray analysis system (Oxford Co.) and a ZAF method was applied for data reduction.

Isotopic analyses of S, Mg, and O were carried out with the Cameca IMS-6f ion microprobes at Arizona State University (ASU) or the University of Tokyo.

Sulfur isotopes were measured with analytical techniques similar to those described in Lin et al. (2005). In brief, a primary Cs^+ beam of 10 kV and ~0.1 nA in intensity was used to excavate 5 to 10 μm crates on the surface of the samples. A normal incidence electron gun was used for charge compensation. Secondary ions ($^{33}S^-$, $^{34}S^-$, $^{36}S^-$, and $^{35}Cl^-$) with a nominal energy of 9 kV were detected with an electron-multiplier-based ion counting system. The mass resolving power was set to ~4500 and both the contribution of $^{32}SH^-$ signal at the center of $^{33}S^-$ signal and that of $^{35}ClH^-$ at the center of $^{36}S^-$ signal were negligible. The sensitivity factor, $\Lambda \equiv (^{35}Cl/^{34}S)/(^{35}Cl^-/^{34}S^-)$, is 0.69 ± 0.05, which was determined using a terrestrial hauyne ($Na_4Ca_{1.6}K_{0.1}Al_6Si_6O_{30}S_{1.8}Cl_{0.07}$) standard. Measured $^{33}S/^{34}S$ isotopic ratios were normalized to that of Canyon Diablo troilite (CDT, $^{33}S/^{34}S$ = 0.17794) (Macnamara and Thode 1950). Mass-independent isotopic anomaly of ^{36}S, $\delta^{36}S$, is derived using the linear mass fractionation correction:

$$\delta^{36}S = \Delta^{36}S + 2 \times \Delta^{33}S \text{ (‰)} \quad (1)$$

where

$$\Delta^{i}S = \left(\frac{^{i}S/^{34}S_{meas}}{^{i}S/^{34}S_{CDT}} - 1 \right) \times 1000 \text{ (‰)} \quad (2)$$

The initial $^{36}Cl/^{35}Cl$ ratio is determined by 100/1.9 × (the slope of the regression line of the $^{35}Cl/^{34}S$ – $^{36}S/^{34}S$ plot) because ^{36}Cl decays into not only ^{36}Cl (1.9%) but also ^{36}Ar (98.1%). Although the $(^{35}Cl^{37}Cl)^{2-}$ signal could be an interference for the $^{36}S^-$ signal and this could make a linear positive correlation between the $^{35}Cl/^{34}S$ ratio and the $^{36}S/^{34}S$ ratio, we can neither separate the $(^{35}Cl^{37}Cl)^{2-}$ signal from the $^{36}S^-$ signal (the required mass resolving power is higher than 120,000) nor determine a production rate of $(^{35}Cl^{37}Cl)^{2-}/^{35}Cl^-$ because Cl has only two isotopes. For this reason, it is important to use terrestrial sodalite to determine the upper limit of the contribution of the $(^{35}Cl^{37}Cl)^{2-}$ signal on the measured $^{36}S^-$ signal.

Magnesium isotopes were measured with a 10 to 20 μm O^- primary ion beam of 12.5 kV and 0.05 to 0.3 nA. Secondary ions with a nominal energy of 10 kV were detected with a Faraday cup (for $^{27}Al^+$ in some measurements) or an electron-multiplier ($^{24}Mg^+$, $^{25}Mg^+$, $^{26}Mg^+$, and $^{27}Al^+$). The mass resolving power was set at ~4000 to eliminate interferences for hydrides or molecular ions to measured Mg isotopes (e.g., $^{24}MgH^+$ and $^{48}Ca^{2+}$). Sensitivity factors, $\Lambda \equiv (^{27}Al/^{24}Mg)/(^{27}Al^+/^{24}Mg^+)$, which were determined with terrestrial minerals are as follows: Λ(spinel) = 1.03 ± 0.02, Λ(fassaïte) = 1.13 ± 0.06, Λ(melilite) = 1.00 ± 0.04, and Λ(anorthite) = 1.15 ± 0.05 for measurements at the University of Tokyo and Λ(spinel) = 1.20 ± 0.01, Λ(melilite) = 1.09 ± 0.01, and Λ(anorthite) = 1.18 ± 0.03 for the measurements at ASU. Because of the absence of an appropriate standard to determine the sensitivity factor for sodalite, we assume Λ(sodalite) = 1.0 in this study. We use $^{25}Mg/^{24}Mg$ = 0.12663 and $^{26}Mg/^{24}Mg$ = 0.13932 as the reference values (Catanzaro et al. 1966). Mass independent isotopic anomaly of ^{26}Mg, $\delta^{26}Mg$, is derived using the linear mass fractionation correction:

$$\delta^{26}Mg = \Delta^{26}Mg - 2 \times \Delta^{25}Mg \text{ (‰)} \quad (3)$$

where

$$\Delta^{i}Mg = \left(\frac{^{i}Mg/^{24}Mg_{meas}}{\text{literature values}} - 1 \right) \times 1000 \text{ (‰)} \quad (4)$$

The initial $^{26}Al/^{27}Al$ ratio is determined by the slope of the regression line of the $^{27}Al/^{24}Mg$ – $^{26}Mg/^{24}Mg$ plot. San Carlos olivine, Burma spinel, Miyakejima anorthite, and synthetic melilite glass were used as standards.

Table 2. ^{36}Cl-^{36}S systematics of CAI#2 sodalite and terrestrial standards.

Phase	Occurrence	$^{35}Cl/^{34}S$ (2σ)	$^{36}S/^{34}S$ (2σ)
CAI#2 sodalite			
#1a	Enclosed[a]	22,129 ± 1297	0.00396 ± 0.00021
#1b	Enclosed	17,915 ± 1624	0.00393 ± 0.00043
#2	Enclosed	10,558 ± 1225	0.00356 ± 0.00027
#3	Isolated[b]	62,582 ± 4967	0.00371 ± 0.00038
#4	Unenclosed[c]	54,928 ± 4789	0.00456 ± 0.00109
#5	Enclosed	42,761 ± 2739	0.00437 ± 0.00036
#6	Enclosed	2620 ± 200	0.00370 ± 0.00024
#7	Unenclosed	105,133 ± 6175	0.00403 ± 0.00040
#8a	Unenclosed	15,217 ± 1451	0.00370 ± 0.00030
#8b	Unenclosed	5442 ± 478	0.00348 ± 0.00014
#9a	Unenclosed	6555 ± 707	0.00374 ± 0.00028
#9b	Unenclosed	3595 ± 370	0.00351 ± 0.00020
#10	Unenclosed	41,216 ± 2611	0.00471 ± 0.00049
Canyon Diablo troilite			
#1		0.00086 ± 0.00006	0.00339 ± 0.00001
#2		0.00049 ± 0.00002	0.00340 ± 0.00001
#3		0.0036 ± 0.0007	0.00339 ± 0.00001
Terrestrial sodalite			
#1		8950 ± 1018	0.00345 ± 0.00014
#2		4721 ± 374	0.00340 ± 0.00010
#3a		6213 ± 469	0.00343 ± 0.00009
#3b		2408 ± 307	0.00350 ± 0.00008
#4		7982 ± 600	0.00351 ± 0.00020
#5		6005 ± 514	0.00346 ± 0.00012
#6		7408 ± 554	0.00336 ± 0.00013
#7		6609 ± 494	0.00349 ± 0.00013
#8		5970 ± 324	0.00339 ± 0.00009
#9		13,186 ± 1078	0.00342 ± 0.00016
#10		6760 ± 519	0.00332 ± 0.00010

[a]A sodalite nodule enclosed by anhedral anorthite.
[b]An isolated sodalite grain.
[c]A sodalite nodule in direct contact with grossular or the CAI rim.

Oxygen isotopes were measured using a 10 kV Cs^+ primary ion beam of ~0.1 nA (10 to 15 μm in diameter). A normal incidence electron gun was used for charge compensation. Secondary O^- ions of 9 kV were collected by a Faraday cup ($^{16}O^-$) or an electron-multiplier ($^{17}O^-$, and $^{18}O^-$). The mass resolving power was set to ~5000 to eliminate the contribution of $^{16}OH^-$ signal at the center of the $^{17}O^-$ signal to less than 1‰. Instrumental mass fractionation was corrected for all the data by repeated measurements of a San Carlos olivine standard ($\delta^{17}O$ = 2.7‰, $\delta^{18}O$ = 5.3‰).

RESULTS

^{36}Cl-^{36}S Systematics of Sodalite in CAI#2

Sulfur isotopic measurements were performed on sodalite in the Na-rich domain and results are listed in Table 2 and plotted in Fig. 2. In this study, we determined the relative sensitivity factor of Cl/S, 0.69 ± 0.05, with a terrestrial hauyne ($[Na,Ca]_{4–8}Al_6Si_6[O,S]_{24}[SO_4,Cl]_{1–2}$). This is different from the previously determined relative sensitivity factor of Cl/S from djerfisherite $[(K,Na)_6(Fe,Ni,Cu)_{25}S_{26}Cl]$ (0.58 in Lin et al. 2005) or from NBS-610 and NBS-612 glasses (0.83 in Hsu et al. 2006). Because the chemical composition of hauyne is very close to that of sodalite ($Na_8Al_6Si_6O_{24}Cl_2$), the newly determined relative sensitivity factor of 0.69 ± 0.05 is a more appropriate one to use. Significant ^{36}S excesses up to ~400‰ were observed in sodalite and they correlate with $^{35}Cl/^{34}S$ ratios. Most data points lie on a single correlation line, suggesting that the ^{36}S excesses are from the decay of ^{36}Cl. However, there are exceptions that indicate variations of ^{36}S excesses in sodalite. The two points with the highest $^{35}Cl/^{34}S$ ratios (CAI#2 sodalite #3 and #7 in Table 2) contain low ^{36}S excesses and do not plot on the correlation line defined by the other data. One of the two points is from the large euhedral isolated sodalite grain located in a hedenbergite-rich cavity (#3 in Fig. 1e) and the other is from a sodalite nodule that exists close to the euhedral isolated sodalite grain. Because these two sodalite grains are not enclosed by anhedral anorthite and are closer to the rim than other sodalite grains measured for S isotopes (Figs. 1d and 1e), it is possible that the observed low ^{36}S excesses in them are a result of isotopic disturbance after sodalite formation.

The inferred initial $^{36}Cl/^{35}Cl$ ratio from CAI#2 sodalite is $(1.4 \pm 0.3) \times 10^{-6}$ (2σ). The observed ^{36}S excesses are not due to any possible contribution from $(^{35}Cl^{37}Cl)^{2-}$, because measurements of terrestrial sodalite under the same analytical conditions yielded no resolvable ^{36}S excesses (inferred $^{36}Cl/^{35}Cl$ ratio is $(0.17 \pm 0.27) \times 10^{-6}$, 2σ). On the other hand, the small ^{36}S excesses ($^{36}Cl/^{35}Cl \sim 0.3 \times 10^{-6}$) observed in the two sodalite grains with the high $^{35}Cl/^{34}S$ ratios overlap with the upper limit of the possible contribution of $(^{35}Cl^{37}Cl)^{2-}$ to ^{36}S.

^{26}Al-^{26}Mg Systematics of Primary and Secondary Phases

Magnesium isotopic measurements were performed on primary phases (spinel, fassaïte, and melilite), the An-Grs domain (anorthite), and the Na-rich domain (anorthite and sodalite). Results are summarized in Fig. 3 and Table 3. Because all the primary phases of CAI#2 have low $^{27}Al/^{24}Mg$ ratios (<8) and the observed ^{26}Mg excesses in primary phases were ~8‰ at most, with the analytical precision of this study we cannot precisely constrain the initial $^{26}Al/^{27}Al$ ratio of the primary minerals (Fig. 3a). Anorthite in the An-Grs domain has significant ^{26}Mg excesses of up to 35‰ (Fig. 3a). These are larger than those of the primary phases. The inferred initial $^{26}Al/^{27}Al$ ratio of anorthite in the An-Grs domain is $(1.2 \pm 0.2) \times 10^{-5}$ (2σ), although the observed data tend to show variations larger than 2σ errors (e.g., anorthite grain #2 in Table 3). In contrast, anorthite and sodalite in the Na-rich domain have no resolvable ^{26}Mg excess (Fig. 3b). Anorthite in the Na-rich domain tends to show higher $^{27}Al/^{24}Mg$ ratio

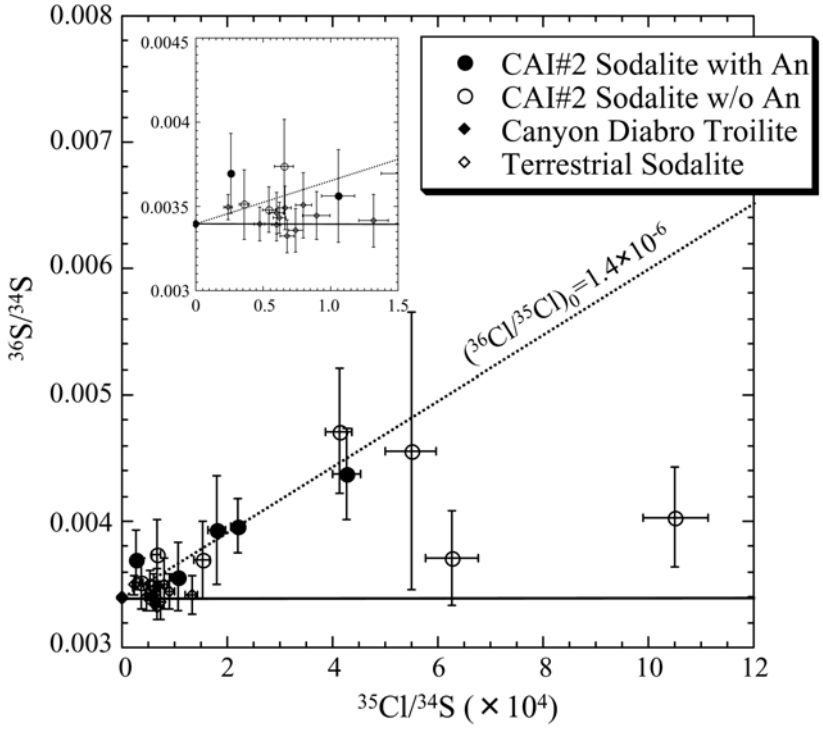

Fig. 2. The $^{35}Cl/^{34}S$-$^{36}S/^{34}S$ plot of sodalite in CAI#2, terrestrial sodalite, and troilite in Canyon Diablo. Sodalite with An indicates sodalite enclosed by anhedral anorthite. Sodalite w/o An indicates sodalite not enclosed by anhedral anorthite. The dashed line is the isochron inferred from data of sodalite in CAI#2, excluding the two points with the highest $^{35}Cl/^{34}S$ ratios. Errors are 2σ.

than that of anorthite in the An-Grs domain (Table 3). Of the two sodalite grains measured, sodalite #1, which is surrounded by anhedral anorthite (Fig. 1d) and contains a significant ^{36}S excess (168 ± 63‰) corresponding to an initial $^{36}Cl/^{35}Cl$ ratio of ~1.4 × 10^{-6}, has a low $^{27}Al/^{24}Mg$ ratio (~1400); sodalite #3, which is the isolated sodalite grain near the CAI rim and has no resolvable ^{36}S excess (94 ± 111‰), shows an $^{27}Al/^{24}Mg$ ratio about 10 times higher (Tables 2 and 3). The upper limit of inferred initial $^{26}Al/^{27}Al$ ratios are 9.4 × 10^{-7}, 4.4 × 10^{-7}, and 2.1 × 10^{-7} (2σ) for anorthite, sodalite #1, and sodalite #3 in the Na-rich domain, respectively.

Oxygen Isotopes of Primary and Secondary Phases

Oxygen isotopic measurements were performed on primary phases (spinel, fassaïte, and melilite), the An-Grs domain (anorthite and grossular), and the Na-rich domain (anorthite and sodalite) (Fig. 4; Table 4). Like in typical Allende CAIs, spinel and fassaïte of CAI#2 are enriched in ^{16}O ($\Delta^{17}O$ ~ –27‰), whereas melilite is relatively ^{16}O-depleted ($\Delta^{17}O$ ~ –6‰). Due to beam overlap, O isotopic measurements of anorthite and grossular in the An-Grs domain sampled both the secondary and primary phases (~5% spinel and ~95% anorthite for the anorthite pit and ~20% fassaïte and ~80% grossular for the grossular pit, respectively). Assuming that the observed O isotopic compositions are the exactly same as mixing ratio of primary and secondary phases, the deduced O isotopic compositions of anorthite and grossular in the An-Grs domain are $\Delta^{17}O$ ~ –12‰ (Table 4). Oxygen isotopic compositions of the Na-rich domain (anorthite and sodalite) are more depleted in ^{16}O ($\Delta^{17}O$ ~ –7‰) than those of the An-Grs domain. All the oxygen isotope data points lie on the carbonaceous chondrite anhydrous mineral (CCAM) line.

DISCUSSION

Implications of ^{36}S Excesses of Sodalite in CAI#2

Large ^{36}S excesses were observed in sodalite of CAI#2 and they correlate linearly with the $^{35}Cl/^{34}S$ ratio (Fig. 2). As noted above, this correlation is not due to the interference of $(^{35}Cl^{37}Cl)^{2+}$ to $^{36}S^{+}$. Although the observed correlation could be explained by a mixing line between a S-rich component with no ^{36}S excess and a S-poor component with ^{36}S excess of larger than 400‰, it is unlikely because such a extreme S isotopic component has not been identified within chondrites (Gao and Thiemens 1993a; Gao and Thiemens 1993b). Therefore, the ^{36}S excesses and their linear correlation with $^{35}Cl/^{34}S$ ratios observed in sodalite of CAI#2 are further evidence for the existence of the short-lived radionuclide ^{36}Cl in the early solar system. Because primary phases of CAIs are depleted in volatile elements, S and especially Cl in CAIs must have been introduced from surroundings when sodalite

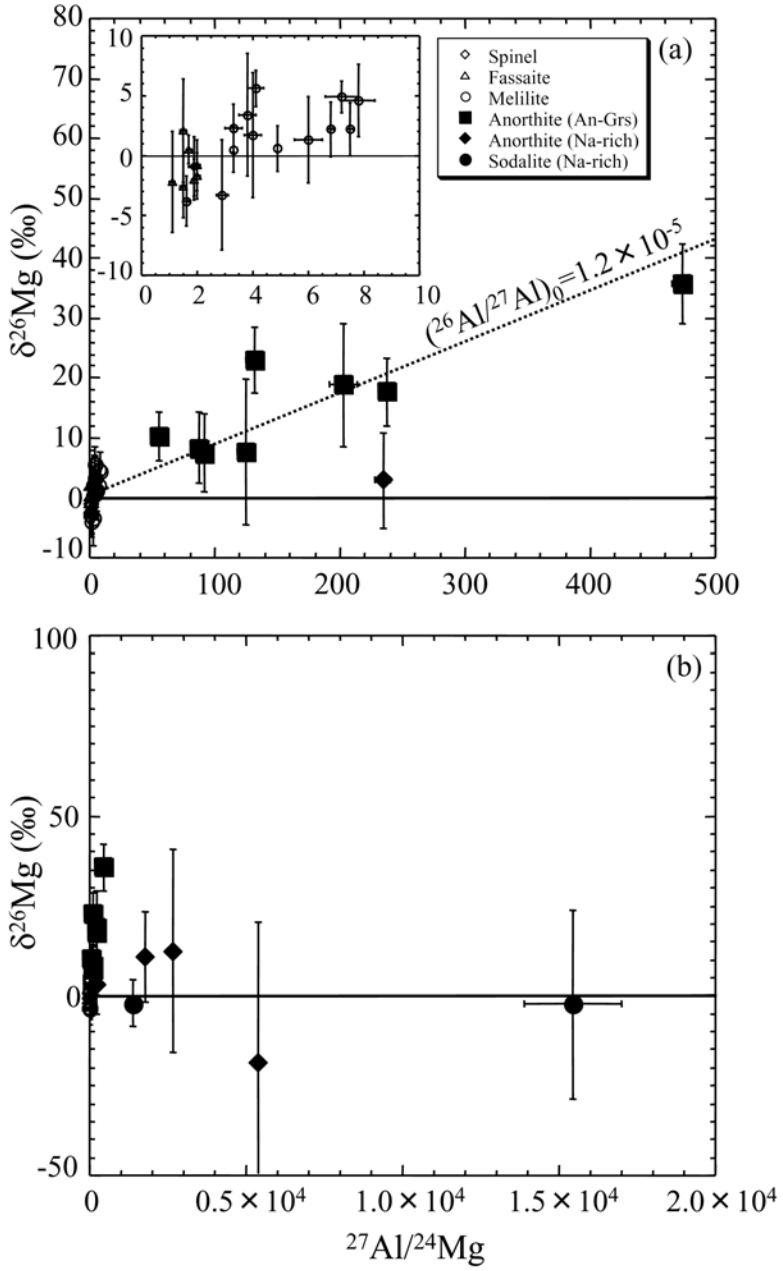

Fig. 3. The $^{27}Al/^{24}Mg$-$\delta^{26}Mg$ plots of primary and secondary minerals in CAI#2. The dashed line in (a) indicates an isochron inferred from data of anorthite in the An-Grs domain. Errors are 2σ.

(or the Na-rich domain) was formed. This indicates that sodalite in CAIs formed while ^{36}Cl was still alive.

We summarize the inferred initial $^{36}Cl/^{35}Cl$ and $^{26}Al/^{27}Al$ ratios of sodalite in CAIs and a chondrule that have been measured for the ^{36}Cl-^{36}S systematics in Table 5 (Lin et al. 2005; Hsu et al. 2006; Plagge et al. 2006; Nakashima et al. 2006; this study). In Table 5, we apply the new sensitivity factor to all the previous results because all the data use sensitivity factors described in Lin et al. (2005) or Hsu et al. (2006). It is evident that the initial $^{36}Cl/^{35}Cl$ ratios of sodalite in CAIs and a chondrule are variable and, interestingly, different $^{36}Cl/^{35}Cl$ ratios were observed in sodalite of CAIs from the same Allende chondrite. The inferred initial $^{36}Cl/^{35}Cl$ ratio of sodalite in Pink Angel (4 to 5×10^{-6}) (Hsu et al. 2006; Nakashima et al. 2006) is higher than that in CAI#2 ($[1.4 \pm 0.3] \times 10^{-6}$). In contrast, no significant ^{36}S excess was observed in sodalite from the Allende fine-grained CAI MP-1 ($<6 \times 10^{-7}$) (Plagge et al. 2006). We also find that the two sodalite grains with the highest Cl/S ratios in CAI#2 contain low ^{36}S excesses that would imply much lower initial $^{36}Cl/^{35}Cl$ ratios if extrapolated as the decay of ^{36}Cl in a closed system.

Table 3. ^{26}Al-^{26}Mg systematics of CAI#2.

Phase	Location	^{27}Al/^{24}Mg (2σ)	^{26}Mg*[a] (2σ)	^{26}Mg/^{24}Mg (2σ)
CAI#2				
Spinel				
#1	In fassaïte	1.9 ± 0.2	–0.9 ± 2.5	0.13920 ± 0.00035
Fassaïte				
#1	Interior	1.5 ± 0.1	2.1 ± 4.3	0.13961 ± 0.00060
#2	Interior	1.7 ± 0.1	0.5 ± 1.2	0.13939 ± 0.00017
#3	Interior	1.9 ± 0.1	–2.0 ± 1.7	0.13904 ± 0.00024
#4	Interior	1.5 ± 0.1	–2.6 ± 2.6	0.13896 ± 0.00037
#5	Near rim	1.1 ± 0.1	–2.2 ± 4.2	0.13901 ± 0.00058
#6	Near rim	2.0 ± 0.1	–0.8 ± 2.1	0.13920 ± 0.00029
#7	Near rim	2.0 ± 0.1	–1.7 ± 1.9	0.13909 ± 0.00026
Melilite				
#1	Interior	2.9 ± 0.2	–3.3 ± 4.6	0.13886 ± 0.00064
#2	Interior	3.8 ± 0.3	3.4 ± 5.1	0.13980 ± 0.00071
#3	Interior	4.0 ± 0.3	1.7 ± 5.2	0.13955 ± 0.00073
#4	Interior	3.3 ± 0.3	2.3 ± 2.0	0.13964 ± 0.00028
#5	Interior	1.6 ± 0.1	–3.8 ± 2.1	0.13879 ± 0.00029
#6	Near rim	6.0 ± 0.5	1.3 ± 3.6	0.13950 ± 0.00051
#7	Near rim	7.8 ± 0.6	4.6 ± 3.0	0.13996 ± 0.00042
#8	Near rim	7.2 ± 0.6	4.9 ± 1.3	0.14000 ± 0.00018
#9	Near rim	4.1 ± 0.3	5.6 ± 1.5	0.14009 ± 0.00020
#10	Near rim	3.3 ± 0.1	0.5 ± 1.9	0.13939 ± 0.00026
#11	Near rim	7.5 ± 0.1	2.2 ± 2.2	0.13963 ± 0.00031
#12	Near rim	6.8 ± 0.1	2.2 ± 2.3	0.13963 ± 0.00032
#13	Near rim	4.9 ± 0.1	0.6 ± 1.9	0.13940 ± 0.00026
Anorthite				
#1	An-Grs	125 ± 7	7.7 ± 12.2	0.14039 ± 0.00170
#2a	An-Grs	56 ± 3	10.3 ± 4.0	0.14076 ± 0.00056
#2b	An-Grs	132 ± 7	23.0 ± 5.4	0.14252 ± 0.00075
#3	An-Grs	203 ± 11	18.9 ± 10.3	0.14195 ± 0.00144
#4	An-Grs	92 ± 5	7.5 ± 6.4	0.14036 ± 0.00090
#5	An-Grs	88 ± 5	8.3 ± 5.9	0.14048 ± 0.00082
#6	An-Grs	473 ± 7	35.7 ± 6.6	0.14430 ± 0.00092
#7	An-Grs	238 ± 6	17.7 ± 5.7	0.14178 ± 0.00079
#8	Na-rich	1792 ± 158	10.8 ± 12.4	0.14083 ± 0.00173
#9a	Na-rich	2667 ± 166	12.4 ± 28.1	0.14105 ± 0.00391
#9b	Na-rich	5374 ± 174	–18.8 ± 39.1	0.13670 ± 0.00545
#10	Na-rich	234 ± 6	2.9 ± 7.9	0.13972 ± 0.00110
Sodalite				
#1	Na-rich	1434 ± 12	–2.0 ± 6.5	0.13904 ± 0.00091
#3	Na-rich	15,445 ± 1554	–2.4 ± 26.2	0.13898 ± 0.00365
Terrestrial				
Spinel		2.5 ± 0.1	–0.2 ± 1.1	0.13930 ± 0.00016
Melilite		6.3 ± 0.1	–0.2 ± 0.9	0.13929 ± 0.00012
Anorthite		457 ± 5	–2.1 ± 3.7	0.13902 ± 0.00052

[a] $\delta^{26}Mg^* = {}^{26}Mg - 2 \times \Delta^{25}Mg$.

Wark (1981) reported alkali-rich halos in the matrix surrounding Allende CAIs, which suggests the outward diffusion of volatiles from CAIs. In such a case, the ^{36}Cl-^{36}S systematics of sodalite in Allende CAIs could be reset and would only preserve information about alteration processes occurring in the Allende parent body, even if sodalite in Allende CAIs formed in the solar nebula. This scenario seems consistent with the fact that sodalite in the Allende CAIs usually does not show any ^{26}Mg excess (Hutcheon and Newton 1981; Hsu et al. 2006; this study), which indicates the ^{26}Al-^{26}Mg systematics of sodalite were closed after ^{26}Al had mostly decayed. However, if sodalite in CAIs only formed during (or the ^{36}Cl-^{36}S systematics were disturbed and completely reset by) an alteration process in the Allende parent body, the initial ^{36}Cl/^{35}Cl ratios of sodalite in the Allende chondrite would show identical values. This is inconsistent with the observed variation of initial ^{36}Cl/^{35}Cl ratios of sodalite in Allende CAIs.

In the Allende chondrite, low initial $^{36}Cl/^{35}Cl$ ratios were observed in sodalite of the fine-grained CAI MP-1 (Plagge et al. 2006) and in sodalite grains that are the closest to the rim of CAI#2 (Figs. 1e and 2). These may be a result of metamorphism in the Allende parent body, resulting in disturbance of the ^{36}Cl-^{36}S systematics. In contrast, sodalite grains that are surrounded by anhedral anorthite in CAI#2 (Fig. 1d) and those in the interior of the large Pink Angel CAI (~2 cm in diameter) (Armstrong and Wasserburg 1981; Hsu et al. 2006) show ^{36}S excesses that linearly correlate with $^{34}S/^{35}Cl$ ratio. These suggest that alteration in the Allende parent body did not completely reset the Cl-S systematics of sodalite. This scenario can explain the existence of ^{36}S excesses in the CAI NQJ1-1#1 from Ningqiang carbonaceous chondrite because CAIs in Ningqiang chondrite are less altered that those from the Allende CV3 chondrite (e.g., Lin and Kimura 2003). The observed variation of initial $^{36}Cl/^{35}Cl$ ratios suggests that sodalite in CAIs has several origins and that their ^{36}Cl-^{36}S systematics have not been reset completely after sodalite formation.

Due to the following two reasons, currently it is difficult to determine the timing of the metamorphism that formed sodalite (and the Na-rich domain) based on the ^{36}Cl-^{36}S systematics. First, we do not know the initial $^{36}Cl/^{35}Cl$ ratio when CAIs first formed. Because Cl is a volatile element and depleted in primary phases of CAIs, it is difficult to determine the initial $^{36}Cl/^{35}Cl$ ratio of primary phases of CAIs. Second, it has been suggested that ^{36}Cl was produced locally in the early solar system. If the ^{36}Cl-^{36}S systematics and the ^{26}Al-^{26}Mg systematics of sodalite in CAIs closed simultaneously, Hsu et al. (2006) concluded that the $^{36}Cl/^{35}Cl$ ratio would have to be on the order of $\sim10^{-2}$ when CAIs were formed ($^{26}Al/^{27}Al \sim 5 \times 10^{-5}$). On this basis, they argued that ^{36}Cl (half-life is 0.3 Myr) had to be decoupled from ^{26}Al (half-life is 0.72 Myr) and that ^{36}Cl was produced by a late episode of energetic particle bombardment in the early solar system because there is no stellar nucleosynthetic source that can produce such a large amount of ^{36}Cl. If this is the case, the production process of ^{36}Cl was localized and distribution of ^{36}Cl abundance in the solar nebula could have been heterogeneous.

It remains a possibility that both ^{36}Cl and ^{26}Al were derived from the same stellar source but only the ^{26}Al-^{26}Mg systematics of sodalite have been reset because the ^{26}Al-^{26}Mg systematics of sodalite are more easily disturbed than the ^{36}Cl-^{36}S systematics. In this case, ^{36}Cl could have been homogeneously distributed in the solar nebula and the observed difference in the initial $^{36}Cl/^{35}Cl$ ratios ($\sim1.4 \times 10^{-6}$ for CAI#2 and 4 to 5×10^{-6} for Ningqiang NQJ1-1#1 and Allende Pink Angel) could indicate an interval of ~0.5 Myr between the sodalite formation in NQJ1-1#1 and Pink Angel and that in CAI#2. Because there is no data about diffusion coefficients of S and Mg in sodalite, we cannot evaluate this possibility now. However, this seems inconsistent with the fact that most secondary phases do not have significant ^{26}Mg excesses (Hutcheon and Newton 1981; Caillet et al. 1993; Davis et al. 1994; MacPherson et al. 1995; Lin et al. 2005; Hsu et al. 2006). Additionally, even if the ^{26}Al-^{26}Mg systematics of sodalite were reset after formation, the inferred initial $^{36}Cl/^{35}Cl$ ratios of 1 to 5×10^{-6} from the three CAIs (NQJ1-1#1, Pink Angel, and CAI#2) should be the lower limit of the initial $^{36}Cl/^{35}Cl$ ratio of the sodalite formation and these values are slightly higher than the production rate of stellar sources ($\sim1 \times 10^{-6}$) (Wasserburg et al. 2006). Thus, the results from this study still support the idea that ^{36}Cl was produced by a late episode of energetic particle bombardment in the early solar system.

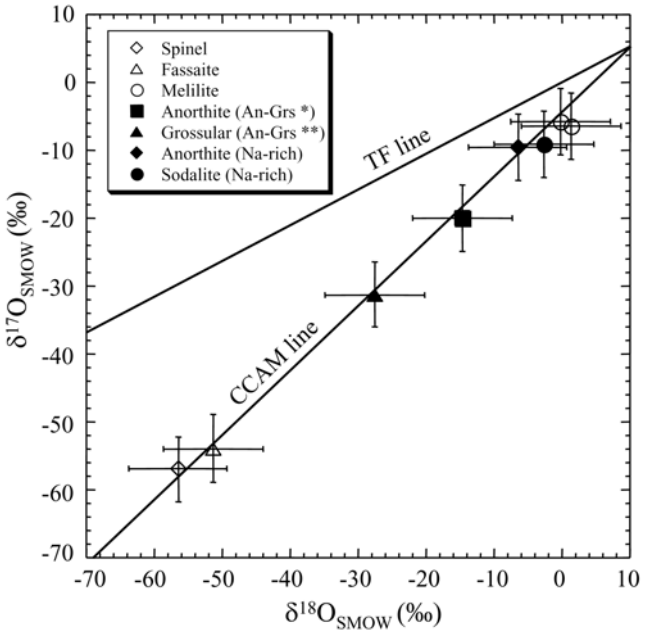

Fig. 4. Oxygen isotopic compositions of individual minerals in CAI#2. Open symbols are primary phases and filled symbols are those of secondary phases. (*): mixture of ~95% anorthite and ~5% spinel. (**): mixture of ~80% grossular and ~20 fassaïte. Errors are 2σ.

Isotopic Heterogeneity of the Two Alteration Domains: Evidence for Multiple Alteration Events

In this study, we found that the An-Grs domain and the Na-rich domain have distinct Mg and O isotopic compositions. In the An-Grs domain, 1) significant ^{26}Mg excesses (up to ~35‰) with an inferred initial $^{26}Al/^{27}Al$ ratio of about 1.2×10^{-5} were observed in anorthite (Fig. 3a) and 2) the estimated O isotopic compositions of anorthite and grossular in the An-Grs domain are ^{16}O-enriched ($\Delta^{17}O \sim -12$‰) (Fig. 4). In contrast, in the Na-rich domain, 1) no resolvable ^{26}Mg excesses (typically <10‰) were observed (Fig. 3b), and 2) O isotopic compositions of anorthite and sodalite in the Na-rich domain are not enriched in ^{16}O ($\Delta^{17}O \sim -7$‰) (Fig. 4).

Table 4. Oxygen isotopic compositions of individual minerals in CAI#2.

Phase	Location	$\delta^{18}O$ (2σ)	$\delta^{17}O$ (2σ)	$\Delta^{17}O$[a] (2σ)
Spinel	Interior	–56.5 ± 7.3	–57.0 ± 4.8	–27.6 ± 6.1
Fassaïte	Interior	–51.4 ± 7.4	–53.9 ± 5.0	–27.2 ± 6.3
Melilite #1	Interior	1.3 ± 7.3	–6.5 ± 4.9	–7.2 ± 6.2
Melilite #2	Interior	–0.2 ± 7.3	–5.7 ± 4.9	–5.6 ± 6.2
An + Sp[b]	An-Grs	–14.7 ± 7.3	–20.0 ± 4.8	–12.3 ± 6.2
(Anorthite)[c]	An-Grs	–12.5 ± 7.7	–18.0 ± 5.1	–11.5 ± 6.5
Grs + Fas[d]	An-Grs	–27.6 ± 7.3	–31.3 ± 4.8	–16.9 ± 6.1
(Grossular)[e]	An-Grs	–18.2 ± 9.3	–21.6 ± 6.1	–12.1 ± 7.8
Anorthite	Na-rich	–6.5 ± 7.3	–9.6 ± 4.9	–6.2 ± 6.2
Sodalite	Na-rich	–2.6 ± 7.3	–9.0 ± 4.9	–7.7 ± 6.2

[a]$\Delta^{17}O = \delta^{17}O - 0.52 \times \delta^{18}O$.
[b]Mixture of ~95% anorthite and ~5% spinel.
[c]Calculated based on mass balance and the spinel data.
[d]Mixture of ~80% grossular and ~20% fassaïte.
[e]Calculated based on mass balance and the fassaïte data.

Table 5. Initial $^{36}Cl/^{35}Cl$ and $^{26}Al/^{27}Al$ ratios of sodalite in CAIs and a chondrule.

Inclusion	Meteorite	Initial $^{36}Cl/^{35}Cl$[a]	Initial $^{26}Al/^{27}Al$	Reference
NQJ1-1#1	Ningqiang	~4.2×10^{-6}	<7×10^{-6}	Lin et al. 2005
Pink Angel	Allende	$(4.5 \pm 1.0) \times 10^{-6}$	<1.7×10^{-6}	Hsu et al. 2006
		$(5.1 \pm 1.7) \times 10^{-6}$		Nakashima et al. 2006
Chondrule	Allende	$(5.1 \pm 1.2) \times 10^{-6}$		Hsu et al. 2006
MP-1	Allende	<6×10^{-7}		Plagge et al. 2006
CAI#2[b]	Allende	$(1.4 \pm 0.3) \times 10^{-6}$	<4.4×10^{-7}	This study

[a]The new sensitivity factor (0.69) of this study is applied.
[b]Sodalite data except for two points with the highest $^{35}Cl/^{34}S$ ratios.

It is interesting that significant ^{26}Mg excesses were observed in anorthite of the An-Grs domain. The An-Grs domain mostly consists of a mixture of fine-grained anorthite and grossular. This texture has been observed in Allende CAIs and AOAs, and is considered to be formed by the decomposition of primary melilite (e.g., Hashimoto and Grossman 1987). The similar texture of the An-Grs domain suggest it could have formed in the same way—by the decomposition of primary phases (mainly melilite).

There are two possibilities to explain the observed ^{26}Mg excesses in secondary anorthite: 1) the alteration process that formed the An-Grs domain occurred while ^{26}Al was still alive, and therefore ^{26}Mg excesses in anorthite in the An-Grs domain are products of the decay of ^{26}Al; 2) the alteration process that formed the An-Grs domain occurred after most of ^{26}Al decayed, but the observed ^{26}Mg excesses were derived from those of precursor primary phases or adjacent primary phases. In the latter scenario, ^{26}Mg excesses in anorthite should not exceed those of primary phases. In addition, there should be no linear correlation between ^{26}Mg excesses and $^{27}Al/^{24}Mg$ ratios. However, the observed ^{26}Mg excesses in anorthite of the An-Grs domain are much larger than those of any primary phases (~8‰ at most) (Fig. 3a) and a linear correlation between ^{26}Mg excesses and $^{27}Al/^{24}Mg$ ratios is observed. These observations are inconsistent with the latter scenario. Assuming a homogeneous ^{26}Al distribution in the early solar system, the inferred initial $^{26}Al/^{27}Al$ ratio of anorthite in the An-Grs domain (~1.2×10^{-5}) indicates that the alteration process that formed the An-Grs domain occurred about 1.5 Myr after CAI formation. This suggests that alteration processes occurred coevally with or even earlier than chondrule formation (6 to 9×10^{-6}) (Kita et al. 2000). In this study, observed ^{26}Mg excesses in one anorthite grain #2 (Table 3) are slightly higher than that the isochron line of the inferred initial $^{26}Al/^{27}Al$ ratio (~1.2×10^{-5}) in the An-Grs domain. This may suggest that the ^{26}Al-^{26}Mg systematics of anorthite in the An-Grs domain were also disturbed by the metamorphism that formed the Na-rich domain and/or occurred in the parent body. If this is the case, the An-Grs domains may have formed less than 1.5 Myr after CAI formation because isotopic disturbances lead to smaller ^{26}Mg excesses in anorthite (e.g., Podosek et al. 1991).

Significant ^{26}Mg excesses have also been observed in secondary phases (anorthite and grossular) in other Allende CAIs (Fagan et al. 2005, 2006). The ^{26}Al-^{26}Mg systematics of secondary phases indicate that alteration processes of CAIs may have occurred in the solar nebula shortly after CAI formation.

The lack of resolvable ^{26}Mg excesses (typically <10‰) and less anomalous O isotopic composition of the Na-rich domain suggest that it was formed by a separate alteration event after the formation of the An-Grs domain. This is consistent with petrologic characteristics of the Na-rich

domain: 1) this domain tends to be closer to the rim of CAI#2 than the An-Grs domain; 2) the abundance of relict primary phases is less than that of the An-Grs domain. Based on petrographic observations, two possible origins of sodalite and nepheline in chondrites have been suggested. One is that they formed by anhydrous metamorphism in the solar nebula (Hashimoto and Grossman 1987; Ikeda and Kimura 1995). The other is that they formed in an asteroidal setting by Na redistribution during fluid-assisted metamorphism (Bridges et al. 1997; Krot et al. 1998). As we previously discussed, the various initial $^{36}Cl/^{35}Cl$ ratios suggest that sodalite in CAIs formed in the solar nebula while ^{36}Cl was alive. However, lower initial $^{36}Cl/^{35}Cl$ ratios observed in sodalite that is fine-grained and/or located near the rim of CAIs suggest the occurrence of a metamorphic process after sodalite formation. We suggest that the observed low or negligible resolvable ^{36}S excess in some sodalite is the result of metamorphism in the parent body that occurred after most ^{36}Cl has decayed.

The upper limits of the inferred initial $^{26}Al/^{27}Al$ ratio for anorthite, sodalite (grain#1) with ^{36}S excesses, and a large euhedral sodalite grain (grain#3) with a small ^{36}S excess in the Na-rich domain are 9.4×10^{-7}, 4.4×10^{-7}, and 2.1×10^{-7}, respectively (Fig. 3b). This implies the ^{26}Al-^{26}Mg systematics in these objects were finally closed at 4.1 Myr, 4.9 Myr, and 5.7 Myr, respectively after CAI formations (assuming the initial $^{26}Al/^{27}Al$ ratio = 5×10^{-5}). Although it has been pointed out that the ^{26}Al-^{26}Mg systematics of some CAIs have been disturbed and Mg isotopic compositions were homogenized by thermal metamorphism (Podosek et al. 1991; MacPherson et al. 1995; LaTourrette and Wasserburg 1998), this is unlikely to explain the low initial $^{26}Al/^{27}Al$ ratio ($<9.4 \times 10^{-7}$) of anorthite in the Na-rich domain because the typical grain size of anorthite in the Na-rich domain is much larger than that of anorthite in the An-Grs domain, which preserves ^{26}Mg excesses (the inferred initial $^{26}Al/^{26}Al$ ratio of $\sim 1.2 \times 10^{-5}$) (Figs. 1b and 2c). The low initial $^{26}Al/^{27}Al$ ratio of anorthite in the Na-rich domain indicates that metamorphism, resulting in the formation of this domain, occurred after the An-Grs domain was formed.

Finally, we note the S and Mg isotopic compositions of sodalite grain#1 in the Na-rich domain. This grain shows a ^{36}S excess (the inferred initial $^{36}Cl/^{35}Cl$ ratio of $\sim 1.4 \times 10^{-6}$) that suggests a nebular origin but no ^{26}Mg excess (the inferred initial $^{26}Al/^{27}Al$ ratio of $<4.4 \times 10^{-7}$). As we mentioned previously, we cannot examine the robustness of the ^{36}Cl-^{36}S systematics and the ^{26}Al-^{26}Mg systematics in sodalite because of the lack of diffusion coefficient of S and Mg isotopes in sodalite. However, if the robustness of the ^{26}Al-^{26}Mg systematics is equal to or better than that of the ^{36}Cl-^{36}S systematics in sodalite, the Mg and S isotopic compositions of sodalite grain#1 suggest that the accretion of planetesimals had to last more than 4 Myr after CAI formation in the early solar system, although this time interval is longer than typical lifetime of circumstellar disks (~3 Myr) (Haisch et al. 2001).

CONCLUSIONS

We measured ^{36}Cl-^{36}S and ^{26}Al-^{26}Mg systematics, and O isotopes of two distinct secondary alteration domains, the An-Grs domain and the Na-rich domain, in a moderately altered type B2 CAI (CAI#2) from the Allende CV3 chondrite. We observed ^{36}S excesses in sodalite of the Na-rich domain. We also observed distinct Mg and O isotopic compositions of the An-Grs and the Na-rich domains.

Significant ^{36}S excesses corresponding to an inferred initial $^{36}Cl/^{35}Cl$ ratio of $\sim 1.4 \times 10^{-6}$ and evidence of late disturbance of the ^{36}Cl-^{36}S systematics were observed in sodalite of the Na-rich domain. However, no resolvable ^{26}Mg excesses were identified in the same sodalite. These are further evidence for the existence of the short-lived radionuclide ^{36}Cl in the early solar system after most of ^{26}Al decayed.

^{36}S excesses in sodalite of CAI#2 mostly correlate with $^{35}Cl/^{34}S$ ratios and the inferred initial $^{36}Cl/^{35}Cl$ ratio of $\sim 1.4 \times 10^{-6}$, but two sodalite grains which are closest to the CAI rim contain low ^{36}S excesses compared to the isochron from other sodalite data. These suggest that sodalite was formed in the solar nebula while ^{36}Cl was still alive, and the ^{36}Cl-^{36}S systematics of sodalite were partly disturbed by a later metamorphism, presumably in the parent body. The high initial $^{36}Cl/^{35}Cl$ ratio of $\sim 1.4 \times 10^{-6}$ suggests that ^{36}Cl was produced by a late episode of energetic particle bombardment in the early solar system, as previously suggested by Hsu et al. (2006).

Distinct Mg and O isotopic compositions of the An-Grs and the Na-rich domains indicate that these domains formed in separate alteration events. Significant ^{26}Mg excesses corresponding to inferred initial $^{26}Al/^{27}Al$ ratios of $\sim 1.2 \times 10^{-5}$ in anorthite of the An-Grs domain indicate that decomposition of primary phases (the An-Grs domain formation) occurred in the solar nebula while ^{26}Al was still alive (within 1.5 Myr after CAI formation). No resolvable ^{26}Mg excesses of anorthite and sodalite in the Na-rich domain suggest that an introduction of volatile elements such as Na and Cl (the Na-rich domain formation) occurred after most ^{26}Al had decayed. Based on the ^{36}Cl-^{36}S systematics in sodalite, this process occurred in the solar nebula while ^{36}Cl was still alive, but a further process occurred after CAIs were embedded in their parent body. The ^{26}Al-^{26}Mg systematics of anorthite and sodalite in the Na-rich domain were finally closed as late as 5.7 Myr after CAI formation.

Acknowledgments–We thank Dr. M. Chaussidon, Dr. A. Hashimoto, and Dr. I. D. Hutcheon for constructive reviews and Dr. C. Floss for thoughtful comments. Chemical composition of terrestrial hauyne was determined by EPMA with the help from Dr. G. Moore at Arizona State University. The terrestrial hauyne standard was provided by Mr. S. Inoue of Hori Mineralogy Ltd., Japan. This study was supported by NASA grant no. NNG05GH37G (L. A. L./Y. G.).

Editorial Handling—Dr. Christine Floss

REFERENCES

Aléon J., Krot A. N., and McKeegan K. D. 2002. Calcium-aluminum-rich inclusions and amoeboid olivine aggregates from the CR carbonaceous chondrites. *Meteoritics & Planetary Science* 37:1729–1755.

Amelin Y., Krot A. N., Hutcheon I. D., and Ulyanov A. A. 2002. Lead isotopic ages of chondrules and calcium-aluminum-rich inclusions. *Science* 297:1678–1683.

Armstrong J. T. and Wasserburg G. J. 1981. The Allende Pink Angel: Its mineralogy, petrology, and the constraints of its genesis (abstract). 12th Lunar and Planetary Science Conference. pp. 25–27.

Bridges J. C., Alexander C. M. O'D., Hutchison R., Franchi I. A., and Pillinger C. T. 1997. Sodium-, chlorine-rich mesostases in Chainpur (LL3) and Parnallee (LL3) chondrules. *Meteoritics & Planetary Science* 32:555–565.

Caillet C., MacPherson G. J., and Zinner E. K. 1993. Petrologic and Al-Mg isotopic clues to the accretion of two refractory inclusions onto the Leoville parent body: One was hot, the other wasn't. *Geochimica et Cosmochimica Acta* 57:4725–4743.

Catanzaro E. J., Murphy T. J., Garner E. L., and Shields W. R. 1966. Absolute isotopic abundance ratios and atomic weights of magnesium. *Journal of Research of the National Bureau of Standards* 70a:453–458.

Clayton R. N. 2003. Oxygen isotopes in the solar system. *Space Science Reviews* 106:19–32.

Clayton R. N., Onuma N., Grossman L., and Mayeda T. K. 1977. Distribution of the pre-solar component in Allende and other carbonaceous chondrites. *Earth and Planetary Science Letters* 34:209–224.

Davis A. M., Simon S. B., and Grossman L. 1994. Alteration of Allende type B1 CAIs: When, where, and how (abstract). 25th Lunar and Planetary Science Conference. pp. 315–316.

Fagan T. J., Guan Y., MacPherson G. J., and Huss G. R. 2005. Al-Mg isotopic evidence for separate nebular and parent-body alteration events in two Allende CAIs (abstract #1820). 36th Lunar and Planetary Science Conference. CD-ROM.

Fagan T. J., Guan Y., and MacPherson G. J. 2006. Al-Mg isotopic constraints on alteration of Allende Ca-Al-rich inclusions (abstract #1213). 37th Lunar and Planetary Science Conference. CD-ROM.

Gao X. and Thiemens M. H. 1993a. Isotopic composition and concentration of sulfur in carbonaceous chondrites. *Geochimica et Cosmochimica Acta* 57:3159–3169.

Gao X. and Thiemens M. H. 1993a. Variations of the isotopic composition of sulfur in enstatite and ordinary chondrites. *Geochimica et Cosmochimica Acta* 57:3171–3176.

Grossman L. 1972. Condensation in the primitive solar nebula. *Geochimica et Cosmochimica Acta* 36:597–619.

Grossman L. 1975. Petrography and mineral chemistry of Ca-rich inclusions in the Allende meteorite. *Geochimica et Cosmochimica Acta* 39:433–454.

Haisch K. E., Jr., Lada E. A., and Lada C. J. 2001. Disk frequencies and lifetime in young clusters. *The Astrophysical Journal* 553: L153–156.

Hashimoto A. and Grossman L. 1987. Alteration of Al-rich inclusions inside amoeboid olivine aggregates in the Allende meteorite. *Geochimica et Cosmochimica Acta* 51:1685–1704.

Hiyagon H. 1998. Distribution of oxygen isotopes in and around some refractory inclusions from Allende (abstract #1582). 29th Lunar and Planetary Science Conference. CD-ROM.

Hsu W., Guan Y., Leshin L. A., Ushikubo T., and Wasserburg G. J. 2006. A late episode of irradiation in the early solar system: Evidence from extinct ^{36}Cl and ^{26}Al in meteorites. *The Astrophysical Journal* 640:525–529.

Hutcheon I. D. and Newton R. C. 1981. Mg isotopes, mineralogy and mode of formation of secondary phases in C3 refractory inclusions (abstract). 12th Lunar and Planetary Science pp. 491–493.

Ikeda Y. and Kimura M. 1995. Anhydrous alteration of Allende chondrules in the solar nebula I: Description and alteration of chondrules with known oxygen isotopic compositions. *Proceedings of the NIPR Symposium on Antarctic Meteorites* 8: 97–122.

Imai H. and Yurimoto H. 2003. Oxygen isotopic distribution in an amoeboid olivine aggregate from the Allende CV chondrites: Primary and secondary processes. *Geochimica et Cosmochimica Acta* 67:765–772.

Kita N. T., Nagahara H., Togashi S., and Morishita Y. 2000. A short duration of chondrule formation in the solar nebula: Evidence from ^{26}Al in Semarkona ferromagnesian chondrules. *Geochimica et Cosmochimica Acta* 64:3913–3922.

Kojima T., Yada S., and Tomeoka K. 1995. Ca-Al-rich inclusions in three Antarctic CO3 chondrites, Yamato-81020 Yamato-82050 and Yamato-790992: Record of low temperature alteration. *Proceedings of the NIPR Symposium on Antarctic Meteorites* 8: 79–96.

Krot A. N., Petaev M. I., Scott E. R. D., Choi B.-G., Zolensky M. E., and Keil K. 1998. Progressive alteration in CV3 chondrites: More evidence for asteroidal alteration. *Meteoritics & Planetary Science* 33:1065–1085.

LaTourrette L. and Wasserburg G. J. 1998. Mg diffusion in anorthite: Implications for the formation of early solar system planetesimals. *Earth and Planetary Science Letters* 158:91–108.

Lin Y., Guan Y., Leshin L. A., Ouyang Z., and Wang D. 2005. Short-lived chlorine-36 in a Ca- and Al-rich inclusion from the Ningqiang carbonaceous chondrites. *Proceedings of the National Academy of Sciences* 102:1306–1311.

Lin Y. and Kimura M. 2003. Ca-Al-rich inclusions from the Ningqiang meteorite: Continuous assemblages of nebular condensates and genetic link to type B inclusions. *Geochimica et Cosmochimica Acta* 67:2251–2267.

Macnamara J. and Thode H. G. 1950. Comparison of the isotopic constitution of terrestrial and meteoritic sulfur. *Physics Review* 78:307–308.

MacPherson G. J., Davis M. A., and Zinner E. K. 1995. The distribution of aluminum-26 in the early solar system—A reappraisal. *Meteoritics* 30:365–386.

McGuire A. V. and Hashimoto A. 1989. Origin of zoned fine-grained inclusions in the Allende meteorite. *Geochimica et Cosmochimica Acta* 53:1123–1133.

Nakashima D., Ott U., and Hoppe P. 2006. Search for extinct ^{36}Cl in Allende CAIs: The Pink Angel (abstract). *Meteoritics & Planetary Science* 41:A129.

Plagge M., Ott U., and Hoppe P. 2006. Search for extinct chlorine-36 in an Allende CAI (abstract #1287). 37th Lunar and Planetary Science Conference. CD-ROM.

Podosek F. A., Zinner E. K., MacPherson G. J., Lundberg L. L., Brannon J. C., and Fahey A. J. 1991. Correlated study of initial ^{87}Sr/^{86}Sr and Al-Mg isotopic systematics and petrologic properties in a suite of refractory inclusions from the Allende meteorite. *Geochimica et Cosmochimica Acta* 55:1083–1110.

Swindle T. D. 1998. Implications of iodine-xenon studies for the timing and location of secondary alteration. *Meteoritics & Planetary Science* 33:1147–1155.

Wark D. A. 1981. Alteration and metasomatism of Allende Ca-Al-

rich materials (abstract). 12th Lunar and Planetary Science Conference. pp. 1145–1147.

Wasserburg G. J., Busso M., Gallino R., and Nollett K. M. 2006. Short-lived nuclei in the early solar system: Possible AGB sources. *Nuclear Physics A* 777:5–69.

Wood J. A. and Hashimoto A. 1993. Mineral equilibrium in fractionated nebular systems. *Geochimica et Cosmochimica Acta* 57:2377–2388.

Yoneda S. and Grossman L. 1995. Condensation of CaO-MgO-Al_2O_3-SiO_2 liquids from cosmic gases. *Geochimica et Cosmochimica Acta* 59:3413–3444.

Young E. D., Simon J. I., Galy A., Russell S. S., Tonui E., and Lovera O. 2005. Supra-canonical $^{26}Al/^{27}Al$ and the residence time of CAIs in the solar protoplanetary disk. *Science* 308:223–227.